Coupled Pacific Rim megadroughts contributed to the fall of the Ming Dynasty's capital in 1644 CE

Article · April 2024

DOI: 10.1016/j.scib.2024.04.029

19 authors, including:

Feng Chen
Yunnan University
145 PUBLICATIONS **2,010** CITATIONS
SEE PROFILE

Tao Wang
Chinese Academy of Sciences
53 PUBLICATIONS **1,118** CITATIONS
SEE PROFILE

Zhao Xiaoen
Yunnan University
16 PUBLICATIONS **42** CITATIONS
SEE PROFILE

Jan Esper
Johannes Gutenberg-Universität Mainz
413 PUBLICATIONS **26,855** CITATIONS
SEE PROFILE

Journal Pre-proofs

Article

Coupled Pacific Rim megadroughts contributed to the fall of the Ming Dynasty's capital in 1644 CE

Feng Chen, Tao Wang, Xiaoen Zhao, Jan Esper, Fredrik Charpentier Ljungqvist, Ulf Büntgen, Hans W. Linderholm, David Meko, Hongna Xu, Weipeng Yue, Shijie Wang, Yujiang Yuan, Jingyun Zheng, Wei Pan, Fidel Roig, Martín Hadad, Mao Hu, Jiachang Wei, Fahu Chen

PII: S2095-9273(24)00263-9
DOI: https://doi.org/10.1016/j.scib.2024.04.029
Reference: SCIB 2714

To appear in: *Science Bulletin*

Received Date: 23 November 2023
Revised Date: 25 March 2024
Accepted Date: 26 March 2024

Please cite this article as: F. Chen, T. Wang, X. Zhao, J. Esper, F. Charpentier Ljungqvist, U. Büntgen, H.W. Linderholm, D. Meko, H. Xu, W. Yue, S. Wang, Y. Yuan, J. Zheng, W. Pan, F. Roig, M. Hadad, M. Hu, J. Wei, F. Chen, Coupled Pacific Rim megadroughts contributed to the fall of the Ming Dynasty's capital in 1644 CE, *Science Bulletin* (2024), doi: https://doi.org/10.1016/j.scib.2024.04.029

Coupled Pacific Rim megadroughts contributed to the fall of the Ming Dynasty's capital in 1644 CE

Feng Chen[a,b*,1], Tao Wang[c,1], Xiaoen Zhao[a,b], Jan Esper[d,e], Fredrik Charpentier Ljungqvist[f,g,h], Ulf Büntgen[i,e,j,k], Hans W. Linderholm[l], David Meko[m], Hongna Xu[n], Weipeng Yue[a], Shijie Wang[a,b], Yujiang Yuan[o], Jingyun Zheng[p], Wei Pan[q], Fidel Roig[r,s], Martín Hadad[t], Mao Hu[a,b], Jiachang Wei[a], Fahu Chen[u,v,w]

[a] *Yunnan Key Laboratory of International Rivers and Transboundary Eco-Security, Institute of International Rivers and Eco-Security, Yunnan University, Kunming 650504, China*

[b] *Southwest United Graduate School, Kunming 650504, China*

[c] *Climate Change Research Center and Nansen-Zhu International Research Centre, Institute of Atmospheric Physics, Chinese Academy of Sciences (CAS), Beijing 100029, China*

[d] *Department of Geography, Johannes Gutenberg University, Mainz 55099, Germany*

[e] *Global Change Research Institute (CzechGlobe), Czech Academy of Sciences, Brno 60300, Czech Republic*

[f] *Department of History, Stockholm University, Stockholm 10691, Sweden*

[g] *Bolin Centre for Climate Research, Stockholm University, Stockholm 10691, Sweden*

[h] *Swedish Collegium for Advanced Study, Linneanum, Thunbergsvägen 2, Uppsala 75238, Sweden*

[i] *Department of Geography, University of Cambridge, Cambridge CB2 3EN, UK.*

[j] *Department of Geography, Faculty of Science, Masaryk University, Brno 61137, Czech Republic.*

[k] *Swiss Federal Research Institute (WSL), Birmensdorf 8903, Switzerland.*

[l] *Regional Climate Group, Department of Earth Sciences, University of Gothenburg, Gothenburg 40530, Sweden*

[m] *Laboratory of Tree-Ring Research, University of Arizona, Tucson AZ 85721, USA*

[n] *Collaborative Innovation Center on Forecast and Evaluation of Meteorological Disasters (CIC-FEMD), Nanjing University of Information Science and Technology, Nanjing 210044, China*

[o] *Key Laboratory of Tree-ring Physical and Chemical Research, Institute of Desert Meteorology, China Meteorological Administration, Urumqi 830002, China*

[p] *Key Laboratory of Land Surface Pattern and Simulation, Institute of Geographical Sciences and*

Natural Resources Research, Chinese Academy of Sciences, Beijing 100101, China

[q] *Key Laboratory of Digital Human Technology R&D and Application of Yunnan Provincial Department of Education, Yunnan University, Kunming 650504, China*

[r] *Laboratorio de Dendrocronología e Historia Ambiental, IANIGLA-CCT CONICET-Universidad Nacional de Cuyo, Mendoza 5500, Argentina*

[s] *Hémera Centro de Observación de La Tierra, Escuela de Ingeniería ForestalFacultad de Ciencias, Universidad Mayor, Huechuraba 8580745, Santiago, Chile*

[t] *Laboratorio de Dendrocronología de Zonas Áridas CIGEOBIO (CONICET-UNSJ), Gabinete de Geología Ambiental (INGEO-UNSJ), San Juan 3306, Argentina*

[u] *ALPHA, State Key Laboratory of Tibetan Plateau Earth System, Environment and Resources (TPESER), Institute of Tibetan Plateau Research (ITPCAS), Chinese Academy of Sciences (CAS), Beijing 100101, China*

[v] *College of Resources and Environment, University of Chinese Academy of Sciences, Beijing 100049, China*

[w] *MOE Key Laboratory of Western China's Environmental System, Lanzhou University, Lanzhou 730000, China*

** Corresponding author, E-mail: feng653@163.com*

[1]*These authors contributed equally to this work.*

Received November 23, 2023; Revised March 25,2024; Accepted March 26, 2024

Abstract

Historical documents provide evidence for regional droughts preceding the political turmoil and fall of Beijing in 1644 CE, when more than 20 million people died in northern China during the late Ming famine period. However, the role climate and environmental changes may have played in this pivotal event in Chinese history remains unclear. Here, we provide tree-ring evidence of persistent megadroughts from 1576-1593 CE and 1624-1643 CE in northern China, which coincided with exceptionally cold summers just before the fall of Beijing. Our analysis reveals that these regional hydroclimatic extremes are part of a series of megadroughts along the Pacific Rim, which not only impacted the ecology and society of monsoonal northern China, but likely also exacerbated external geopolitical and economic pressures. This finding is corroborated by last millennium reanalysis and numerical model simulations revealing internally driven Pacific sea surface temperature variations and the predominance of decadal scale La Niña-like conditions to be responsible for precipitation decreases over

northern China, as well as extensive monsoon regions in the Americas. These teleconnection patterns provide a mechanistic explanation for reoccurring drought spells during the late Ming Dynasty and the environmental framework fostering the fall of Beijing in 1644 CE, and the subsequent demise of the Ming Dynasty.

Keywords: Paleoclimate; Beijing; Precipitation reconstruction; Climate-society interactions; Tree rings; Ming Dynasty

1. Introduction

Megadrought is the climatic phenomenon that typically coincides with major ecological and societal impacts and commonly influences large regions for many years [1-5]. Numerous studies have recently demonstrated the importance of megadroughts to human wellbeing, and how these extreme and persistent climate states may have contributed to the restructuring or even demise of ancient civilizations in the Mediterranean [6], Western Asia [7-9], Khmer [10], Mesoamerica [11,12], and southwestern United States [1]. With Beijing as its capital, the Chinese empires held sway over large areas of continental eastern Asia during diverse climates from the 13th to the early 20th centuries. These political units were based on agricultural societies depending on precipitation and its predictable seasonality to provide food for large and growing populations [13]. They were therefore vulnerable to changes in the amount and distribution of precipitation on different timescales, particularly during periods when additional political factors weakened authorities [14,15]. Although megadroughts are documented in Chinese historical records, the limited number of high-resolution climate observations prior to the 20th century in Asia has resulted in a controversy about the onset, duration, intensity, and causes of these megadroughts [16-19].

The late Ming Dynasty (1573-1644) has been described as affected by severe droughts and cold periods as well as socio-economic crises including military failures, political corruption, famine, and plague [13-15,18,19]. Over the past two decades, a number of climate reconstructions and climate model simulations have been used to investigate possible mechanisms triggering and sustaining late Ming Dynasty droughts [14,16-18,20], but two major uncertainties remain [2,17]. First, how the the cold temperatures during the climax of the Little Ice Age (LIA, ca. 1570–1710) interact with weakening of the East Asian summer monsoon (EASM) during this period, and which mechanism and external forcings were responsible for triggering the megadrought [17,21-23]. Second, new hydroclimatic records showed a consistency in the spatial pattern of megadroughts controlled by natural variability from the 1570s to the 1640s in the monsoon region of eastern China, although the region is mainly controlled by contrasting North-South rainfall patterns on interannual scales. Uncertainties in the spatial pattern of megadroughts on interdecadal scales still exist [2,13,24,25]. This temporal variability and large-scale covariance suggest a more complex relationship between East Asian monsoon precipitation and external forcing factors than is commonly apprehended.

Despite substantial research, the spatio-temporal pattern and driving mechanism of late Ming Dynasty megadrought remained elusive [14]. It particularly has not been established why these megadroughts persisted that long what the mechanisms of extreme precipitation variations were in northern monsoonal China. To fill this gap, we present a new high-resolution precipitation reconstruction covering Beijing derived from a tree-ring widths network from 1550–2022 CE. We benchmark the new reconstruction against regional and large-scale paleoclimatic and historical evidence. Our results delineate the timing and amplitude of Beijing precipitation anomalies, as well as the potential causes of coupled megadroughts on the Pacific Rim during the late Ming Dynasty.

2. Data and methods

2.1. Tree ring and precipitation data

183 cores from 91 pine trees (*Pinus tabuliformis* Carr.) were sampled at six sites within the greater Beijing region during September 2022. Samples were fine-sanded to facilitate tree-ring identification, which is important in slow-growing pines, and annual ring widths were measured to the nearest 0.001 mm. Due to the high mean correlation between the master chronology and each individual ring-width series across all six sites (*Rbar* = 0.51, $P < 0.01$), a regional mean chronology was developed. The 183 ring-width series were standardized by calculating ratios from negative exponential curves and combined into a regional chronology (RCH) using a robust mean. The Beijing RCH was correlated with instrumental precipitation data to assess the seasonal response of tree-ring data. Principal component analysis was used to extract common drought signals for northern China integrating three tree-ring records [26-28], and the HJZ chronology and Beijing RCH (Table S1). The first principal component (PC1) from this network explains 44.2% of the total variance of regional ring width data with from 1570–2012 CE. Monthly instrumental precipitation totals recorded at the Beijing station since 1914 CE, and gridded monthly precipitation data from 1901–2021 covering 39.5°N–41°N and 115.5°E–117.5°E (CRU TS4.06) [29] were used for calibration.

2.2. Precipitation reconstruction

After identifying the seasonal precipitation forcing from previous-year August to current-year July, a linear regression was employed to develop the Beijing precipitation reconstruction. Split calibration-verification [30] was applied to assess the stability of the relationships from 1914–2022 and prevent overfitting. The fully replicated precipitation reconstruction exceeds an expressed population signal (EPS) [31] of 0.85 at a sample depth of six trees back to 1550 CE.

Megadrought periods were identified based on the criterion of the 11-year running mean deviating from the 1550–2022 mean continuously for more than 10 years. We focussed on those megadroughts exceeding the 50th percentile. Correlations against CRU gridded precipitation data were performed to assess the spatial representation of

the reconstruction. We compared PC1 of the reconstructed precipitation with drought reconstructions from the Pacific Rim [1,2] to evaluate the occurrence of spatially coupled megadroughts. To explore the possible forcing mechanisms of such events, correlations between the new Beijing precipitation reconstruction and gridded global sea surface temperatures (SST) [32] were computed. To evaluate the probability of exceptional NDVI [33] values during late Ming Dynasty megadrought periods, cumulative distribution functions (CDFs) were applied to tree-ring derived June-August NDVI estimates.

2.3. Model data

We used monthly output of three models from the fourth Paleoclimate Model Intercomparison Project (PMIP4) of last millennium runs including INM-CM4-8, MIROC-ES2L, and MRI-ESM2-0 [34]. These models share common orbital, solar, volcanic, land use/land cover changes, greenhouse gas forcings and cover the pre-industrial millennium from 850-1849 CE [34]. We also used monthly output from 12 all-forcing runs of the Community Earth System Model-Last Millennium Ensemble (CESM-LME) project (https://www.cesm.ucar.edu/community-projects/lme) [35].

2.4 CAM5 experimental design

We used the Community Atmosphere Model (CAM5), which is the atmospheric component of the Community Earth System Model (CESM, more detailed information can be found at https://www.cesm.ucar.edu/models/cam), to perform two additional simulations. The configuration set "F_1850_CAM5" was selected and the horizontal resolution set to 2.5° longitude × 1.9° latitude and 26 vertical hybrid levels. Due to minor aerosol influences during the period 1550–1850, the chemical process module was turned off to improve computational efficiency. The first simulation is the LIA control simulation. The monthly climatological SST and ice boundary conditions were constructed from the 1550–1849 runs of the PMIP4 MRI-ESM2-0 last millennium simulation. Atmospheric greenhouse gas concentrations were set to the average 1550–1850 CE values (CO_2 = 278.7575 ppm, CH_4 = 728.7289 ppb, N_2O = 272.5540 ppb, 1 ppm = 1000 ppb) according to the PMIP4 forcing data. The second simulation is an anomalous SST sensitivity simulation. SST anomalies were derived by computing residuals from the LIA period Last Millennium Reanalysis data [32]. We then imposed these SST anomalies on the monthly climatological SSTs of the control run. The greenhouse gases concentrations for the sensitivity simulation were set to the average values from 1576–1643 CE (CO_2 is 278.2289 ppm, CH_4 is 707.4775 ppb, N_2O is 271.3893 ppb, 1 ppm = 1000 ppb). The orbital forcing was set to the 1850 values for both simulations. The two simulations were consecutively integrated over 40 years, though the results represent averages over only 30 years to allow CAM5 to attain a relative equilibrium state over 10 years. Due to the minimal difference in greenhouse gas concentrations between the two experiments, differences likely reflect the changing boundary SSTs conditions during the period of 1576–1643. While volcanic aerosols are

equally important for drought formation, the lag and interannual influence of volcanic eruptions are stronger [16,36]. Therefore, we focus on the dominant role of the Pacific SST background and related mechanisms in the onset of the Pacific Rim megadrought during the late Ming Dynasty.

3. Results

We present an August-July precipitation reconstruction from 1550–2022 CE derived from a network of common pine (*Pinus tabuliformis* Carr.) sites within 100 km of Beijing (Fig. 1; Table S1 online). These pines are severely water-limited and their radial growth is well correlated with precipitation, moisture availability (scPDSI) and grassland productivity (Normalized Difference Vegetation Index (NDVI)) (Fig. S1 online). The reconstruction explains ~41.7% of the variance in the instrumental precipitation from 1914–2022 CE and passes all split-sample calibration-verification tests (Table S2 online). At a mean and standard deviation (σ) of 508 mm and 92 mm, respectively, our precipitation reconstruction shows multi-decadal dry periods from the 1570s to the 1640s, commonly associated with the climax of the LIA, followed by a prolonged pluvial period until 1709, coinciding with the collapse of the Ming and transition to the Qing Dynasties (Table S3 online) [14].

Together with a new quantitative precipitation reconstruction, we assessed the duration and severity of historically documented megadroughts [18,25]: the so-called Wanli megadrought from 1576–1593 CE and the Chongzhen megadrought from 1624–1643 CE during which mean precipitation reached only 413 and 399 mm, respectively. The severity and duration of these megadroughts recorded in the new Beijing precipitation reconstruction far exceed any other event. Moreover, nine (the mean is 294 mm) of the eleven (the mean is 287 mm) driest years, during which precipitation was smaller 2σ, fall within the Wanli and Chongzhen megadroughts. When considering additional tree-ring records beyond the Beijing region, we find evidence that the Wanli and Chongzhen megadroughts extended as far away as Shaanxi [26], Henan [27], and Shanxi [28] (Figs. 1 and 2). These latter records are completely independent of our precipitation reconstruction and thereby verifying their accuracy. Meanwhile, persistent droughts occurred in the southwestern North America and the Altiplano region of South America, both of which were accompanied by cold weather [37] (Fig. 3). Unlike northern China, the upper southwestern North America experienced more drought events from the 1570s to the early 1640s, but on an interdecadal scale consistent with the late Ming megadrought. Records from different sources, such as cave stalagmites and ice core records from the Pacific Rim, are likewise indicative of hydroclimatic anomalies during the 1576-1644 CE [38-41].

Although the correlation between variables can vary over different time periods, the Pacific SST variability is likely to exert some important influences on the Beijing precipitation (Fig. 1b). A similar correlation pattern is observed using the PC1 of the tree-ring network (Fig. S2e online). Notably, compared with the entire LIA interval, the

tropical central and eastern Pacific show La Niña-like SST anomalies during the period of 1576–1643 CE considering latest Last Millennium Reanalysis data (Fig. 4a) [42], while in contrast, SSTs at mid-to-low latitudes in the western Pacific show positive anomalies. Additionally, the mid- and high-latitude regions of the North Pacific and the eastern Pacific at mid-latitudes show significant negative SST anomalies, resembling the Victoria mode [43]. Concurrently, the Indian Ocean basin-scale SSTs show warming anomalies, while North Atlantic SSTs show a significant negative anomaly.

4. Discussion and conclusions

4.1. Megadrought and societal vulnerability of the late Ming Dynasty

The command system of the Ming Dynasty covered the whole of monsoonal northern China and was linked to the main military fortresses within the vast administrative regions of the Great Wall, which spans more than 8,000 kilometers. By the late 16th century, it had become a convoluted political and economic network. The political and military infrastructures of the monsoon fringe areas were internally interdependent, resistant to lower-level environmental changes, vulnerable to failures of the EASM [14,18]. The inter-regional megadroughts reported here, corresponding with the climax of the LIA [37] appear to have weakened the political and economic resilience against environmental stressors. Harvest failure likely affected financial coping strategies, and increased the difficulty and cost of the Ming government to maintain their military presence on the northern frontier of the empire, and contributed to the collapse of the Ming Dynasty as the largest empire in East Asia [14,44,45].

Several studies showed that the combination of persistent water shortage and food insecurity caused by poor harvests had cascading consequences on the resilience and functioning of the socioecological systems of the Ming Dynasty [14,20,46]. Our precipitation reconstruction demonstrates that sustained megadroughts coincided with a period of weakened monsoon strength. Reduced economic productivity and decreased availability of energy in monsoonal northern China occurred when agricultural productivity was reduced by the effects of megadrought. Whereas the vast desert grassland of monsoonal northern China is widely distributed within the modern 200 mm/a and 350 mm/a precipitation isohyets (Fig. 1a) [47,48]. During the two megadrought periods of the late Ming Dynasty, these isohyets migrated southward by 200–300 km into the Beijing area so that the growth, of several principal grain crops was unable to be sustained in the arid regions adjacent to the Great Wall [20] (Fig. 2). Fairly rapid but sustained environmental changes forced the migration of several species within the ecosystem including grassland rodents, with serious consequences for Beijing inhabitants and the cores (nine garrisons, 九边重镇) of the northern defence line of the Ming Dynasty (Fig. 1a). The ecological balance of the entirety of monsoonal northern China was disrupted and manifested by the outbreaks of the Wanli and Chongzhen epidemics that spread over to neighbouring areas in the 1580s (Fig. 1c) and fostered the migration of rodents during extreme drought [20, 49].

Subsequent to environmental changes and damages, the megadroughts accelerated the dysfunction of the imperial political and economic systems and contributed to the collapse of the social order [14]. The destruction of military farms and land acquisition led to the complete collapse of the supply system of government troops in monsoonal northern China and significantly reduced the self-sufficiency of military administrative regions, which necessitated an increased transfer of funds from the central government [50,51]. During the period from the 1570s to the 1580s, military expenditure accounted for almost 76% of total government spending, and frequent wars exacerbated the national financial crisis [14,50,51]. In an attempt to mitigate this fiscal crisis, the Ming government raised the taxation levels, which in turn forced increasing numbers of people to become refugees and eventually led to a large-scale peasant uprising at Shaanxi, the opposite end of the empire [51,52]. The worsening fiscal situation of the Ming government, which was increasingly unable to afford the greatly increased military and civil expenditure and frequently defaulted on military salaries and rations, resulted in a decline of military effectiveness. Many officers and soldiers were dismissed and even rebelled, the most famous being Zicheng Li (1606–1645), who ultimately overthrew the rule of the Ming Dynasty. The decades of weakened monsoonal rainfall in northern China likely triggered harvest failure, which must be regarded as the key socioeconomic stressor during the late Ming Dynasty.

In addition to the internal socioeconomic problems, the Ming Dynasty also faced major geopolitical pressures including frequent wars in regions surrounding the empire, such as the conflict with Japan from 1592 to 1598 [53,54] and the escalating conflict among the Manchus starting in 1618 [55,56]. These wars caused the empire to incur enormous financial, human, and material costs. Studies indicate a linkage between the fall of the Ming Dynasty and a decrease in silver imports [57,58]. Whereas there is no direct evidence linking silver production to drought, these coupled megadroughts undoubtedly impacted silver producing regions in South America (Fig. 3) [5], and there were also continuous wars and severe famines in Europe during this period [59,60]. “Seventeenth-century crisis” and the decline in silver production prevented the Ming Dynasty from obtaining enough silver, and leaded to a sharp rise in food prices [57,58,61]. Unlike the collapse of ancient civilizations and the implicated climate crisis [6-9,11,12], the Ming Dynasty, with its vast area, diverse climates and territories, and complex systems, fell due to the coupled influences of megadrought and unrelenting geopolitical factors during the early age of exploration.

4.2. Causes of coupled megadroughts-a moldel perspective

Changes in oceanic boundary conditions contributed to the development of anomalies in large-scale atmospheric circulation and monsoon systems. During the 1576–1643 period large-scale SST anomalies were likely the principal cause of the coupled megadroughts on the Pacific Rim. Assessment of CAM5 model series simulations (see Data and methods) revealed distinct climatic changes during the boreal summer (May–September) in the East Asia. These include significantly decreased sea-

level pressure in low-latitude land areas and coastal regions of Asia from 1576–1643 (Fig. 4b). Negative 500 hPa geopotential height anomalies developed in East Asia (Fig. 4c), indicative of a substantially weakened influence of the western Pacific subtropical high in eastern China and causal for persistent cyclonic circulation anomalies in the lower troposphere over southern China (Fig. 4d). Anomalously northerly winds over southeastern China signified the weakening of the East Asian summer monsoon, disrupting inter-regional water vapour transport (Fig. S3) and caused a dipole summer precipitation pattern including negative deviations in northern and positive deviations in southern China (Fig. 4e). In this process, the La Niña-like cold SST anomalies can lead to the weakening and southward shifting of the Intertropical Convergence Zone, which can also contribute to weakening the East Asian summer monsoon [62]. Additionally, the cold SST anomalies in the central equatorial Pacific Ocean and warm SST anomalies in the western North Pacific Ocean also hindered the development of the Philippine anomalous anticyclone [63], explaining the weakened influence of the subtropical high on eastern China. At the same time, precipitation in the North American monsoon region were significantly decreased.

The 1576–1643 SST anomalies also appear to be linked to constrained monsoonal rainfall in the Pacific Rim including the southern United States and Mexico (Fig. 4e). However, these changes in the North American monsoon circulation are insignificant (Fig. 4d). The main reason for decreased monsoonal precipitation are the La Niña-like cold SST anomalies, which lead to a decrease in mid- and low-tropospheric temperatures in the tropical North American region (Fig. S4). This in turn caused a significant reduction in atmospheric water vapor content and an anomalous moisture reduction in the North American monsoon region (Fig. S5).

During the austral summer (November–March), the South American summer monsoon is significantly enhanced in response to significant SST decreases in the eastern tropical Pacific Ocean (Fig. S6). Water vapor transport from the tropical Atlantic to South America increases significantly, leading to a pronounced convergence of moisture in central tropical South America and substantial enhancement of monsoon rainfall. However, along the western coastal regions of South America, the La Niña-like anomalies appear to have forced a significant decline in atmospheric moisture content and reduction in monsoon rainfall along the western coastal regions of South America. These changes in precipitation are consistent with paleoclimate records that indicate simultaneous droughts in northern China and the American monsoon regions along the Pacific Rim during this period [1,5].

Both external forcing factors and internal variability of the climate system can have a significant impact on SSTs during this period. In this study, additional assessment of past millennium simulations from the CESM-LME project and PMIP4 multi-models shows that None of the existing simulations or ensemble of simulations can reproduce these SST anomalies, in particular the La Niña-like cold SST anomalies and Victoria-like mode in the Pacific driven by transient external forcing (Figs. S7–S9

online). This suggests that the co-occurring megadroughts in the Pacific Rim region were caused by the anomalous Pacific SSTs, which probably caused by internal variability rather than externally driven. Furthermore, in Western North America and South America studies have similarly found that ocean-atmosphere variability has played an important role in driving past megadroughts [2,5,64]. Certainly, we also have to admit that the current model performance still has significant shortcomings, especially in simulating the climate of East Asia, and there is an urgent need for improvement to better understand the mechanisms of precipitation changes.

Beijing has thrived for centuries, and it has developed into one of the largest urban agglomerations in the world [65]. However, due to its geographical location and huge urban water consumption, it is still threatened by drought and water scarcity [66]. Although precipitation in Beijing has decreased only slightly over the past 40 years, the frequency and severity of drought have increased significantly due to the impact of global warming [67,68,69]. To alleviate the water shortage in northern China, the Chinese government has constructed the world's largest water diversion project. However, a relatively dry period during the late Ming Dynasty occurred in the Hanjiang river basin (Fig. 2) [70], which is the source area of the South to North Water Diversion. Despite the inconsistent trends in hydroclimatic changes in the Han River Basin and northern China since the 20th century caused by anthropogenic forcing and natural variability. If a similar megadrought would reoccur presently, the efficiency of these water transfer facilities would almost certainly be greatly reduced. Therefore, future water resource planning of Beijing must fully consider the impact of extreme events.

Conflict of interest

The authors declare that they have no conflict of interest.

Acknowledgements

This work was supported by Basic Science Center for Tibetan Plateau Earth System (BSCTPES, 41988101) and National Natural Science Foundation of China (32061123008). Ulf Büntgen and Jan Esper were supported by the ERC Advanced Grant Monostar (AdG 882727) and the Czech Science Foundation(23-08049S, HYDRO8). Fredrik Charpentier Ljungqvist was supported by the Swedish Research Council (Vetenskapsrådet, 2018-01272) and the Marianne and Marcus Wallenberg Foundation (MMW 2022-0114), and he conducted this work as a Pro Futura Scientia XIII Fellow funded by the Swedish Collegium for Advanced Study through the Riksbankens Jubileumsfond. We greatly appreciate the comments of Kevin Anchukaitis.

Data availability

The precipitation reconstruction is downloaded from the Mendeley Data Repository Center (https://doi.org/10.17632/c95f8nn9c3.2).

Author contributions

Feng Chen and Tao Wang designed the research, performed the analysis, drafted and revised the manuscript, Feng Chen and Tao Wang contributed equally. All the authors provided comments and revised the manuscript. All the authors have read and approved the final version of the manuscript.

References

[1] Williams AP, Cook ER, Smerdon JE, et al. Large contribution from anthropogenic warming to an emerging North American megadrought. Science 2020; 368: 314-318.

[2] Steiger NJ, Smerdon JE, Seager R, et al. ENSO-driven coupled megadroughts in North and South America over the last millennium. Nat Geosci 2021; 14: 739-744.

[3] Fuentealba M, Bahamóndez C, Sarricolea P, et al. The 2010–2020'megadrought'drives reduction in lake surface area in the Andes of central Chile (32º-36ºS). J Hydrol-Reg Stud 2021; 38: 100952.

[4] Ionita M, Dima M, Nagavciuc V, et al. Past megadroughts in central Europe were longer, more severe and less warm than modern droughts. Commun Earth Environ 2021; 2: 61.

[5] Morales MS, Cook ER, Barichivich J, et al. Six hundred years of South American tree rings reveal an increase in severe hydroclimatic events since mid-20th century. Proc Natl Acad Sci USA 2020; 117: 16816-16823.

[6] Weiss H. Megadrought and collapse: from early agriculture to Angkor. Oxford 2017; 93-160.

[7] Weiss, H. Pyramid building and collapse. Proceedings of the Proc Natl Acad Sci USA 2022; 119: e2212483119.

[8] Watanabe TK, Watanabe T, Yamazaki A, et al. Oman corals suggest that a stronger winter shamal season caused the Akkadian Empire (Mesopotamia) collapse. Geology 2019; 47: 1141-1145.

[9] Manning SW, Kocik C, Lorentzen B, et al. Severe multi-year drought coincident with Hittite collapse around 1198–1196 BC. Nature 2023; 614: 719-724.

[10] Buckley BM, Anchukaitis KJ, Penny D, et al. Climate as a contributing factor in the demise of Angkor, Cambodia. Proc Natl Acad Sci USA 2020; 107: 6748-6752.

[11] Haug GH, Gunther D, Peterson LC, et al. Climate and the collapse of Maya civilization. Science 2003; 299: 1731-1735.

[12] Fedick SL, Santiago LS. Large variation in availability of Maya food plant sources during ancient droughts. Proc Natl Acad Sci USA 2022; 119: e2115657118.

[13] Ge Q, Zheng J, Hao Z, et al. Recent advances on reconstruction of climate and extreme events

in China for the past 2000 years. J Geogr Sci 2016; 26: 827-854.

[14] Zheng J, Xiao L, Fang X, et al. How climate change impacted the collapse of the Ming dynasty. Clim Change 2014; 127: 169-182.

[15] Peng Y, Shen C, Cheng H, et al. Modeling of severe persistent droughts over eastern China during the last millennium. Clim Past 2014; 10: 1079-1091.

[16] Chen K, Ning L, Liu Z, et al. One drought and one volcanic eruption influenced the history of China: The late Ming Dynasty mega-drought. Geophys Res Lett 2020; 47: e2020GL088124.

[17] Zhao J, Cheng H, Yang Y, et al. Role of the summer monsoon variability in the collapse of the Ming Dynasty: Evidences from speleothem records. Geophys Res Lett 2021; 48: e2021GL093071.

[18] Cook ER, Anchukaitis KJ, Buckley BM, et al. Asian monsoon failure and megadrought during the last millennium. Science 2010; 328: 486-489.

[19] Bai M, Zheng J, Hao Z, et al. Hydroclimate patterns over the Northern Hemisphere when megadroughts occurred in North China during the last millennium. Clim Change 2019; 157: 365-385.

[20] Chen F, Martín H, Zhao X, et al. Abnormally low precipitation-induced ecological imbalance contributed to the fall of the Ming Dynasty: new evidence from tree rings. Clim Change 2022; 173: 13.

[21] Liu Y, Cai W, Sun C, et al. Anthropogenic aerosols cause recent pronounced weakening of Asian Summer Monsoon relative to last four centuries. Geophys Res Lett 2019; 46: 5469-5479.

[22] Held IM, Soden BJ. Robust responses of the hydrological cycle to global warming. J Clim 2006; 19: 5686-5699.

[23] Zhao J, Cheng H, Cao J, et al. Orchestrated decline of Asian summer monsoon and Atlantic meridional overturning circulation in global warming period. Innov Geosci 2023; 100011.

[24] Li Q, Deng Y, Wang S, et al. A half-millennium perspective on recent drying in the eastern Chinese Loess Plateau. Catena 2022; 212: 106087.

[25] Zheng J, Wang WC, Ge Q, et al. Precipitation variability and extreme events in eastern China during the past 1500 years. Terr Atmos Ocean Sci 2006; 17: 579.

[26] Chen F, Opała-Owczarek M, Owczarek P, et al. Summer monsoon season streamflow variations in the middle Yellow River since 1570 CE inferred from tree rings of *Pinus tabulaeformis*. Atmosphere-Basel 2020; 11: 717.

[27] Zhang Y, Tian Q, Guillet S, et al. 500-yr. precipitation variability in Southern Taihang Mountains, China, and its linkages to ENSO and PDO. Clim Change 2017; 144: 419-432.

[28] Li Q, Deng Y, Wang S, et al. A half-millennium perspective on recent drying in the eastern Chinese Loess Plateau. Catena 2022; 212: 106087.

[29] Harris I, Osborn TJ, Jones P, et al. Version 4 of the CRU TS monthly high-resolution gridded multivariate climate dataset. Sci Data 2020; 7(1): 109.

[30] Meko DM, Graybill DA. Tree-ring reconstruction of Upper Gila River discharge. J Am Water Resour Assoc 1995; 31: 605-616.

[31] Wigley TM, Briffa KR, Jones PD. On the average value of correlated time series, with applications in dendroclimatology and hydrometeorology. J Appl Meteorol Climatol 1984; 23: 201-213.

[32] Rayner NAA, Parker DE, Horton EB, et al. Global analyses of sea surface temperature, sea ice, and night marine air temperature since the late nineteenth century. J Geophys Res-Atmos 2003; 108: 4407.

[33] Pinzon JE, Tucker CJ. A non-stationary 1981-2012 AVHRR NDVI3g time series. Remote Sens-Basel 2014; 6: 6929-6960.

[34] Jungclaus JH, Bard E, Baroni M, et al. The PMIP4 contribution to CMIP6-Part 3: The last millennium, scientific objective, and experimental design for the PMIP4 past1000 simulations. Geosci Model Dev 2017; 10: 4005-4033.

[35] Otto-Bliesner BL, Brady EC, Fasullo J, et al. Climate variability and change since 850 CE: An ensemble approach with the Community Earth System Model. Bull Am Meteorol Soc 2016; 97: 735-754.

[36] Mann ME, Steinman BA, Brouillette DJ, et al. Multidecadal climate oscillations during the past millennium driven by volcanic forcing. Science 2021; 371: 1014-1019.

[37] Büntgen U, Allen K, Anchukaitis KJ, et al. The influence of decision-making in tree ring-based climate reconstructions. Nat Comm 2021; 12: 3411.

[38] Black DE, Abahazi MA, Thunell RC, et al. An 8-century tropical Atlantic SST record from the Cariaco Basin: Baseline variability, twentieth-century warming, and Atlantic hurricane frequency. Paleoceanography 2007; 22.

[39] Duan W, Cai B, Tao T, et al. Multi-timescale variations of $\delta^{18}O$-$\delta^{13}C$ in stalagmites: insights into isotopic disequilibrium and human activities. J Geophys Res-Atmos 2023; 128: e2023JD039607.

[40] Thompson LG, Mosley-Thompson E, Davis ME, et al. Annually resolved ice core records of tropical climate variability over the past~ 1800 years. Science 2013; 340: 945-950.

[41] Zhang P, Cheng H, Edwards RL, et al. A test of climate, sun, and culture relationships from an 1810-year Chinese cave record. Science 2008; 322: 940-942.

[42] Tardif R, Hakim GJ, Perkins WA, et al. Last Millennium Reanalysis with an expanded proxy database and seasonal proxy modelling. Clim Past 2019; 15: 1251-1273.

[43] Bond NA, Overland JE, Spillane M, et al. Recent shifts in the state of the North Pacific. Geophys Res Lett 2003; 30(23): 2183.

[44] Tian F, Chen X, Su Y. Comparative Analysis of Extreme Drought Events and Social Impacts in Henan Province during the Middle Ming Dynasty. Weather Clim Soc 2022; 14: 1009-1021.

[45] Liu Q, Li G, Kong D, et al. Climate, disasters, wars and the collapse of the Ming Dynasty. Environ Earth Sci 2018; 77: 1-15.

[46] Pederson N, Hessl AE, Baatarbileg N, et al. Pluvials, droughts, the Mongol Empire, and modern Mongolia. Proc Natl Acad Sci USA 2014; 111: 4375-4379.

[47] Liang E, Shao X, Liu H, et al. Tree-ring based PDSI reconstruction since AD 1842 in the Ortindag Sand Land, east Inner Mongolia. Sci Bull 2007; 52: 2715-2721.

[48] Zhang LS, Fang XQ, Ren GY, et al. Environmental changes in the North China farming-grazing transitional zone. Earth Sci Front 1997; 4: 127-134.

[49] Brook T. Comparative pandemics: the Tudor-Stuart and Wanli-Chongzhen years of pestilence, 1567-1666. J Glob Hist 2020; 15: 363-379.

[50] Swope KM. The Military Collapse of China's Ming Dynasty. Routledge 2014; 1618-44.

[51] Xiao L, Fang X, Zheng J, et al. Famine, migration and war: Comparison of climate change impacts and social responses in North China between the late Ming and late Qing dynasties. The Holocene 2015; 25: 900-910.

[52] Han J, Yang Y. The socioeconomic effects of extreme drought events in northern China on the Ming dynasty in the late fifteenth century. Clim Change 2021; 164: 26.

[53] Swope JKM. The three Great Campaigns of the Wanli Emperor, 1592-1600: Court, military, and society in late sixteenth-century China. University of Michigan; 2001.

[54] Lewis JB. The East Asian War, 1592-1598: International Relations, Violence and Memory. Routledge 2014.

[55] Cui J, Chang H, Burr GS, et al. Climatic change and the rise of the Manchu from Northeast China during AD 1600-1650. Clim Change 2019; 156: 405-423.

[56] Zhang DD, Jim CY, Lin GC, et al. Climatic change, wars and dynastic cycles in China over the last millennium. Clim Change 2006; 76: 459-477.

[57] Bakewell PJ. Registered silver production in the Potosí district, 1550-1735. Jahrbuch für Geschichte Lateinamerikas 1975; 12: 67-103.

[58] Atwell W S. Another look at silver imports into China, ca. 1635-1644. J World Hist 2005; 467-489.

[59] Ljungqvist FC, Seim A, Collet D. Famines in medieval and early modern Europe – Connecting climate and society. Wires Clim Change 2024; 15, e859

[60] Barragán R, Zagalsky PC. Potosí in the Global Silver Age (16th-19th Centuries). Brill; 2023.

[61] Von Glahn R. Myth and reality of China's seventeenth-century monetary crisis. J Econ Hist 1996; 56: 429-454.

[62] Yang B, Kang S, Ljungqvist FC, et al. Drought variability at the northern fringe of the Asian summer monsoon region over the past millennia. Clim Dyn 2014; 43: 845-859.

[63] Wang B, Wu R, Fu X. Pacific–East Asian teleconnection: how does ENSO affect East Asian climate?. J Clim, 2000; 13(9): 1517-l1536.

[64] Coats S, Smerdon JE, Cook BI, et al. Internal ocean-atmosphere variability drives megadroughts in Western North America. Geophys Res Lett 2016; 43: 9886-9894.

[65] Liu Y, Ou C, Li Y, et al. Regularity of rural settlement changes driven by rapid urbanization in North China over the three decades[J]. Sci Bull 2023; 68(18): 2115-2124.

[66] He C, Liu Z, Wu J, et al. Future global urban water scarcity and potential solutions. Nat Commun 2021; 12: 4667.

[67] Chen FH, Xie TT, Yang YJ, et al. Discussion of the "warming and wetting" trend and its future variation in the drylands of Northwest China under global warming. Sci China Earth Sci 2023; 66: 1241-1257.

[68] Yao L, Lu J, Jiang H, et al. Satellite-derived aridity index reveals China's drying in recent two decades. Iscience 2023; 26: 106185.

[69] Büntgen U, Crivellaro A, Arseneault D, et al. Global wood anatomical perspective on the onset of the Late Antique Little Ice Age (LALIA) in the mid-6th century CE. Sci Bull 2022; 67: 2336-2344.

[70] Chen F. Role of Pacific Ocean climate in regulating runoff in the source areas of water transfer projects on the Pacific Rim. Mendeley Data 2024, V2, doi: 10.17632/pksym6cjfg.2

Fig. 1. Precipitation reconstruction for Beijing. (a) Map of the study area, showing the

location of the tree-ring sites and climate station. The tree-ring series for Beijing is correlated with the gridded precipitation dataset for total August–July precipitation over northern China for the period 1914–2021. Note the positive correlation between RC chronology and gridded precipitation dataset over the North China Plain. (b) Spatial plots of correlations between sea surface temperature (SST) [32] and the tree-ring series for Beijing for the period 1870–2022. (c) Reconstructed total August–July precipitation (1550–2022 CE). Shown are green (precipitation > 508 mm) and brown (precipitation < 508 mm) bars with an 11-year running average (black line) centered on the average of the precipitation reconstruction (horizontal black line). The Wanli and Chongzhen pandemics are indicated by black vertical bars [48], and the uncertain of the precipitation is shown in gray (±1 standard deviation). (d) Regional dry/wet index series for the North China Plain, Jiang-Huai area, Jiang-Nan area, and central eastern China during the period 1550-1995, derived from a yearly drought/flood grade dataset [13]. (e)The 50-year and 100-year running variance changes in reconstructed precipitation. (f) Plot of the running expressed population signal (EPS) and the sample size of the RC chronology for Beijing

Fig. 2 Moisture-sensitive tree-ring records from northern China. (a) Beijing precipitation reconstruction (this study), (b) tree-ring width series of the HJZ site, (c) tree-ring width series of the WTS site [24], (d) precipitation reconstruction from the southern Taihang Mountains [27], (e) gridded PDSI reconstruction for our study area [15] and (f) streamflow reconstruction for the Hanjiang River [68]. The Wanli and Chongzhen megadroughts are indicated by red vertical bars. The bold line represents smoothing with an 11-year running average. The inset figure shows precipitation variation during the different periods: full-length (1550–2022) and two driest periods 1576–1593 and 1624-1643.

Fig. 3. Regional hydroclimate records on the Pacific Rim from 1570 to 1644. (a) The pathways of political, financial, and social factors leading to the fall of the Beijing. The inset figures show cumulative distribution functions (CDFs) of NDVI, silver production of Potosi and annual China warfare frequency [55,59]. CDFs plotted for different periods: full-length (1550–2022), instrumental (1981–2015), and two driest periods 1576–1593 and 1624-1643. Smooth lines are lognormal fits to CDFs. Annotated are probabilities of not exceeding the mean $NDVI_{1981\text{-}2015}$. (b) Reconstructed SST anomalies (unit: ºC) during the period 1576–1643 compared to the mean of the period 1550–1850. The numbers 1, 2, 3 and 4 denote the late Ming rebellions, the Ming-Manchu war of 1618-1683, the East Asian War of 1592–1598 and the Thirty Years War 1618–1648, respectively. (c) Beijing precipitation reconstruction (this study), (d) PC1 of several tree-ring records [26-28], HJZ chronology and Beijing chronology, (e) summer soil moisture reconstruction for southwestern North America [1], (f) drought reconstruction for the Altiplano region of South America [5] and (g) Northern Hemisphere summer temperature reconstruction [37]

Fig. 4. Reconstructed SST and simulated climate changes. (a) Reconstructed SST anomalies (unit: ºC) during the period of 1576–1643 compared to the mean of the period 1550–1850. CAM5 simulated differences of (b) sea level pressure (unit: hPa), (c) geopotential height at 500 hPa (unit: m), (d) wind field at 850 hPa (units: m s^{-1}), and (e) precipitation (unit: mm d^{-1}) during boreal summer (May–September) between the sensitivity simulation and control simulation. Areas with statistical significance exceeding the 90% confidence level are denoted by dots or grey shading.

Feng Chen is a professor of physical geography at Institute of International Rivers and Eco-Security, Yunnan University. He is a dendrochronologist, paleoclimatologist, and global change ecologist. His research interest focuses on paleoclimate and the evolution of human civilization.

Tao Wang is a professor and the executive deputy director of the Climate Change

Research Center at the Institute of Atmospheric Physics, Chinese Academy of Sciences. He obtained his Ph.D. degree from Institute of Atmospheric Physics, Chinese Academy of Sciences. His research interest focuses on paleoclimate modeling and decadal climate change.

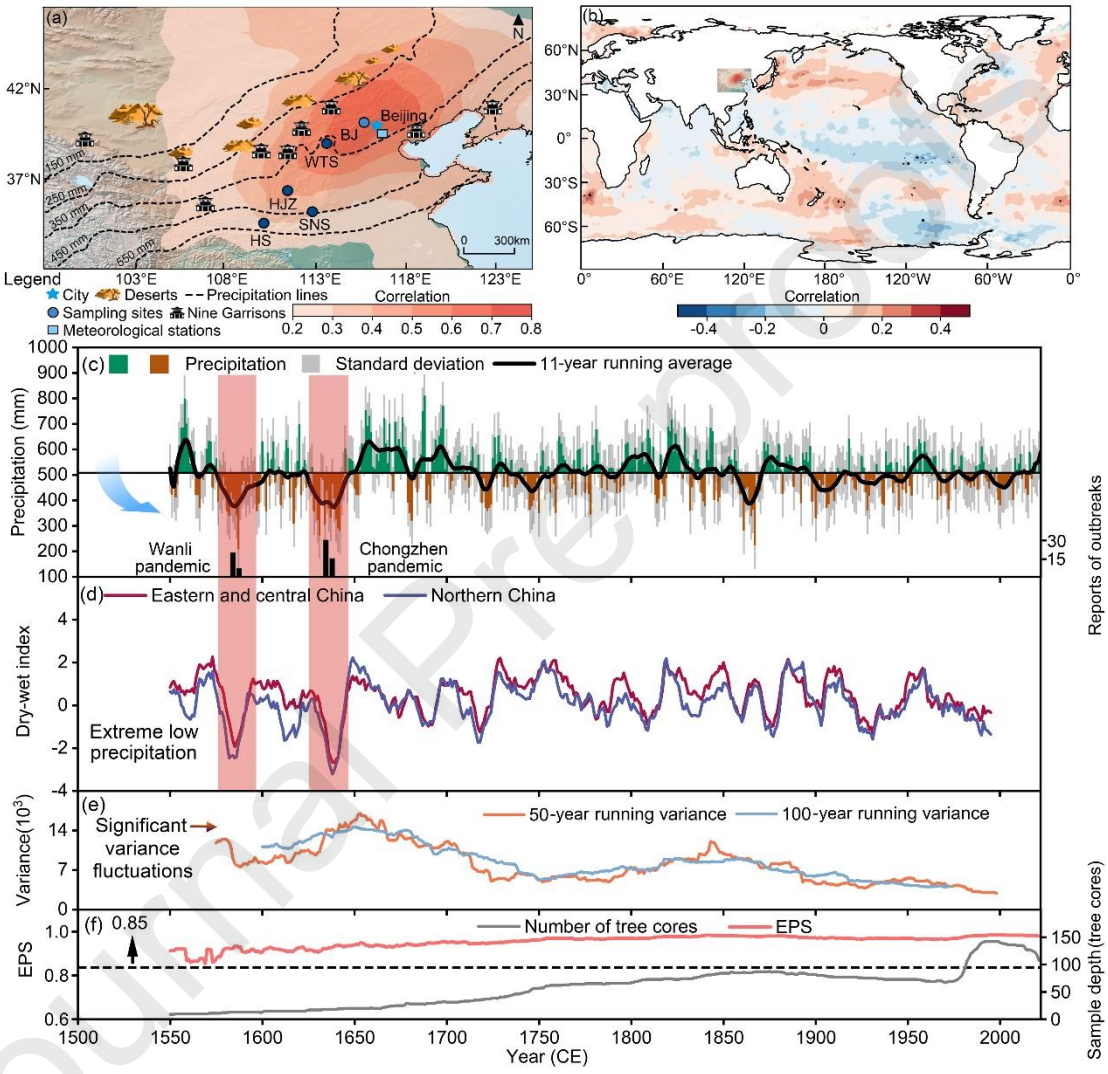

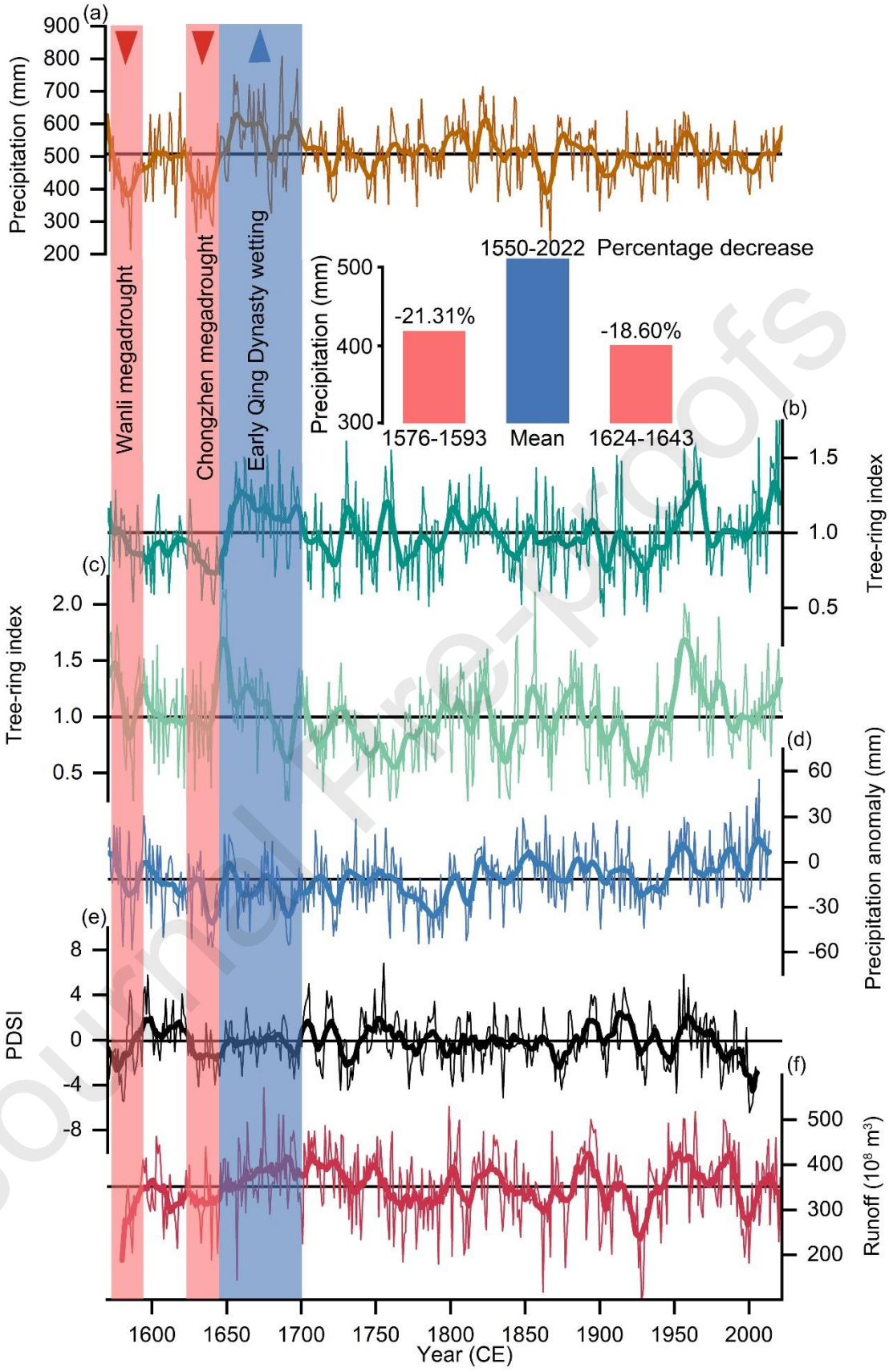
(a)
Precipitation (mm)
900
800
700
600
500
400
300
200
Wanli megadrought
Chongzhen megadrought
Early Qing Dynasty wetting
1550-2022 Percentage decrease
Precipitation (mm)
500
400
300
-21.31%
-18.60%
1576-1593
Mean
1624-1643
(b)
Tree-ring index
1.5
1.0
0.5
(c)
Tree-ring index
2.0
1.5
1.0
0.5
(d)
Precipitation anomaly (mm)
60
30
0
-30
-60
(e)
PDSI
8
4
0
-4
-8
(f)
Runoff (10^8 m^3)
500
400
300
200
1600
1650
1700
1750
1800
1850
1900
1950
2000
Year (CE)